

Appearance Matching Adapter for Exemplar-based Semantic Image Synthesis

Siyoon Jin¹ Jisu Nam² Jiyoung Kim¹ Dahyun Chung¹ Yeong-Seok Kim³
 Joonhyung Park³ Heonjeong Chu³ Seungryong Kim²
¹Korea University ²KAIST ³Hyundai Mobis

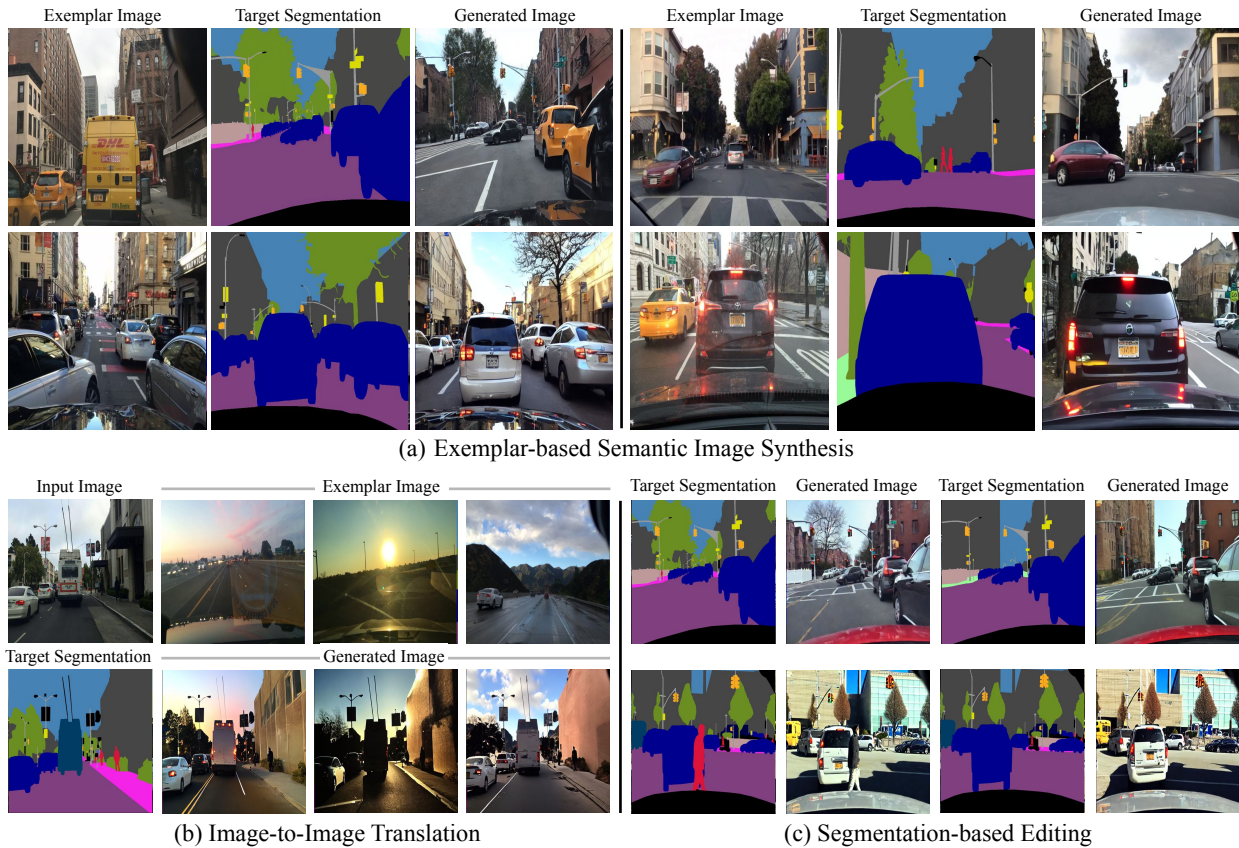


Figure 1. **AM-Adapter enables Exemplar-based Semantic Image Synthesis.** (a) Given an exemplar image representing the user-intended appearance and a target segmentation map guiding the semantic structure, our **AM-Adapter** generates high-quality images that preserve the detailed local appearance of the exemplar and maintain the accurate image structure defined by the segmentation map. We demonstrate the versatility of our method in various applications, including (b) image-to-image translation and (c) segmentation-based image editing.

Abstract

Exemplar-based semantic image synthesis aims to generate images aligned with given semantic content while preserving the appearance of an exemplar image. Conventional structure-guidance models, such as ControlNet, are

limited in that they cannot directly utilize exemplar images as input, relying instead solely on text prompts to control appearance. Recent tuning-free approaches address this limitation by transferring local appearance from the exemplar image to the synthesized image through implicit cross-image matching in the augmented self-attention mechanism

of pre-trained diffusion models. However, these methods face challenges when applied to content-rich scenes with significant geometric deformations, such as driving scenes. In this paper, we propose the Appearance Matching Adapter (AM-Adapter), a learnable framework that enhances cross-image matching within augmented self-attention by incorporating semantic information from segmentation maps. To effectively disentangle generation and matching processes, we adopt a stage-wise training approach. Initially, we train the structure-guidance and generation networks, followed by training the AM-Adapter while keeping the other networks frozen. During inference, we introduce an automated exemplar retrieval method to efficiently select exemplar image-segmentation pairs. Despite utilizing a limited number of learnable parameters, our method achieves state-of-the-art performance, excelling in both semantic alignment preservation and local appearance fidelity. Extensive ablation studies further validate our design choices. Code and pre-trained weights will be publicly available.: <https://cvlab-kaist.github.io/AM-Adapter/>

1. Introduction

Semantic image synthesis [15, 16, 25, 27, 29, 38, 40, 43, 44] aims to generate an image aligned with given semantic content (e.g., segmentation maps) while faithfully reflecting user-defined visual attributes (e.g., styles, lighting, or object details). This task is critical for various downstream applications, including autonomous driving [6], medical imaging [46], and virtual/augmented reality (AR/VR) [8].

Recent advances in structure-guidance methods [15, 29, 44] such as ControlNet have been prominent in this field. These methods allow fine-grained spatial control by integrating an additional encoder into pre-trained text-to-image (T2I) diffusion models, while adjusting visual appearance based on text prompts (e.g., ‘realistic’ or ‘nighttime’). However, despite their promising structural control, as shown in Figure 2(a), they often fail to capture user-defined visual details, as text descriptions alone are insufficient to convey fine-grained visual information.

To overcome this limitation, several approaches have explored exemplar-based semantic image synthesis for visual conditioning [1, 18, 41], leveraging pre-trained image encoders such as CLIP [32]. This is typically achieved by mapping the exemplar’s features from the encoder onto the pre-trained T2I diffusion model using linear projection heads [7, 17, 30, 39, 41]. However, as shown in Figure 2(b), these models still struggle to accurately transfer local appearances from exemplars, as global mappings via linear layers are insufficient for embedding complex visual features into generation models.

To resolve these, some studies [1, 2, 18, 26] have focused on local appearance transfer through hand-crafted attention control in the self-attention modules of pre-trained diffusion

models. Prior works [2, 26] achieve this through augmented self-attention, which provides the key and value matrices of the exemplar image to the self-attention mechanism that synthesizes a new image aligned with the given semantic content. This can be interpreted as finding correspondences between the synthesized and exemplar images through implicit matching between query and key matrices, then warping the exemplar’s appearance based on the corresponding value matrices. These methods effectively transfer the local appearances of exemplars to the synthesized image in a constrained setting. However, as presented in Figure 2(c), they rely on implicit matching within the self-attention mechanism, leading to inaccurate results under large geometric deformations in content-rich, complex scenarios (e.g., driving scenes). This further causes inconsistent correspondences across different categories (e.g., cars matched to buildings, trees matched to roads), ultimately producing blurry or distorted outputs. Recent approaches [1, 18, 26] address this by applying additional constraints to enhance the attention signal, but they remain limited to foreground objects, hindering their applicability in complex scenarios.

The most straightforward solution to improve these approaches may be to directly fine-tune the augmented self-attention module to improve matching. However, this is challenging as the module needs to learn both matching and generation simultaneously, ultimately resulting in an unstable training signal and overfitting, which will be discussed in Figure 9(d). Although recent studies [11] attempted to fine-tune such a model, they are typically constrained to specific domains, such as foreground-centric human videos [12].

To this end, we present a novel method that combines the spatial control capabilities of structure-guidance model [29] with effective local appearance transfer via learnable appearance matching control. We introduce the Appearance Matching Adapter (AM-Adapter), which enhances implicit matching within the augmented self-attention of pre-trained diffusion models by integrating semantic information from segmentation maps (Figure 2(d)). Built on a frozen pre-trained diffusion model and ControlNeXt [29], the adapter focuses solely on enhancing matching, effectively disentangling generation from matching to maximize performance.

Our network architecture consists of two branches: an *Appearance Net*, which extracts local appearance from a given exemplar image and segmentation map, and a *Structure Net*, which synthesizes a target image from random noise, aligned with a new target segmentation map. To harness the semantic relationship between exemplar and target images for improved matching, we first construct a categorical matching cost between the exemplar and target segmentation maps, which is then concatenated with the implicit matching cost in the self-attention module. To find locally consistent matches within the 4D space between the exem-

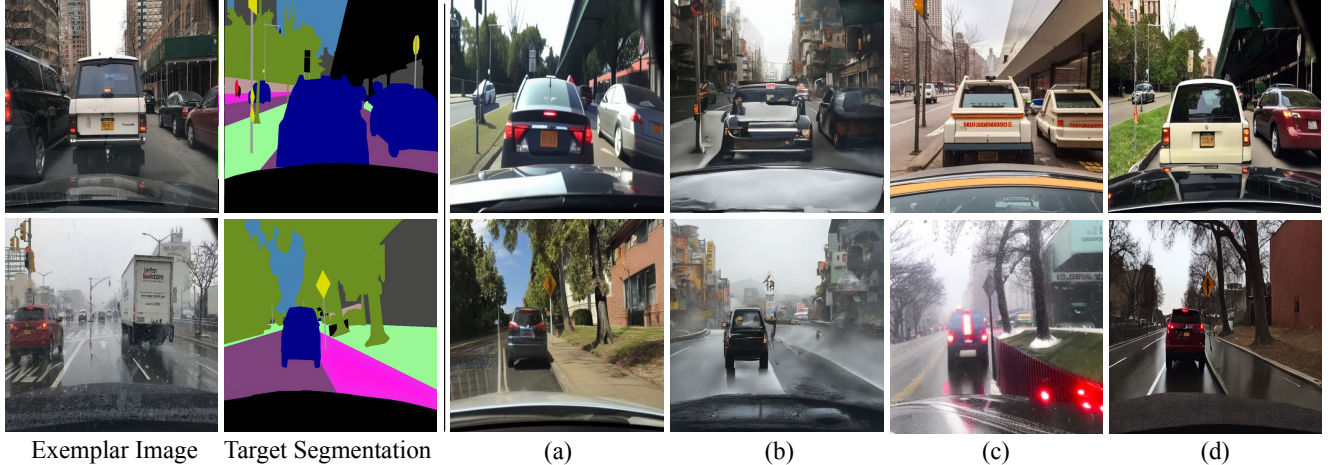


Figure 2. **Effectiveness of our AM-Adapter:** semantic image synthesis results by (a) ControlNeXt [29], (b) IP-Adapter [41] + ControlNet [43], (c) Ctrl-X [18], and (d) **AM-Adapter**. Compared to prior studies that often fail to capture local exemplar’s appearance or struggle with finding accurate matching between exemplar image and target segmentation, our AM-Adapter precisely matches exemplars to targets in content-rich scenarios, preserving local details while maintaining alignment with the target structure.

plar and target, we refine the combined cost using a 4D cost aggregation module. The final output is added residually to the original implicit matching cost to stabilize training.

To further disentangle generation and matching, we adopt a stage-wise training approach. First, we pre-train the diffusion model and ControlNeXt [29] on the target domain, and then train the matching adapter while keeping the diffusion model and ControlNeXt frozen. This approach is highly efficient, as it only requires updating the matching adapter’s parameters, preserving the image quality and structural consistency of the pre-trained models.

During inference, previous studies [1, 18] manually select exemplar images, which may be labor-intensive in a specific setting. To address this, we propose an automatic exemplar retrieval method that selects exemplar image-segmentation pairs from a large pool to maximize matchable regions with the synthesized target image.

Despite the limited number of learnable parameters, our method achieves state-of-the-art performance in complex segmentation-to-image tasks, such as driving scenes [4, 42]. Extensive ablation studies validate the effectiveness of each component, and we demonstrate the versatility of our model across various downstream applications, as in Figure 1.

2. Related Work

Semantic Image Synthesis. Semantic Image Synthesis [15, 16, 25, 27, 29, 38, 43, 44] aims to generate images that align with given semantic structures while accurately reflecting user-defined visual appearance. Several structure-guided models [15, 16, 25, 29] provide structural guidance using a learnable spatial encoder integrated into the pre-trained diffusion model and control global appearance through text prompts. However, these models often fail to

capture user-defined appearance details, as they do not incorporate exemplar images, and text descriptions alone are insufficient to depict fine-grained details in the images.

Exemplar-based Semantic Image Synthesis. Several studies [7, 17, 30, 39, 41] have leveraged pre-trained image encoders, such as CLIP [32], to extract image features from a given exemplar and project them into compact embeddings, often through linear projection layers. While these methods achieve promising results in specific domains, they fail to preserve local appearance in content-rich scenes, like driving scenes, since they focus on global appearance.

Recent studies address this with hand-crafted attention control, typically by shifting keys and values of the exemplar image into the self-attention module of the synthesized target image. This transfers the exemplar value, which includes appearance information, into the target structure based on the implicit matching cost between the target query and exemplar key. Several methods [1, 18, 26] enhance this implicit matching cost by using intermediate diffusion features [26], spatially-aware appearance transfer [18], or attention map contrasting [1]. While these approaches improve over implicit matching alone, performance remains limited by the inherent matching accuracy of self-attention, which is still constrained to foreground-centric objects and struggles to find precise matches in content-rich images.

3. Method

3.1. Preliminaries

Diffusion models typically adopt a UNet architecture [33] composed of an encoder and a decoder. Each block within this consists of self-attention layers and cross-attention lay-

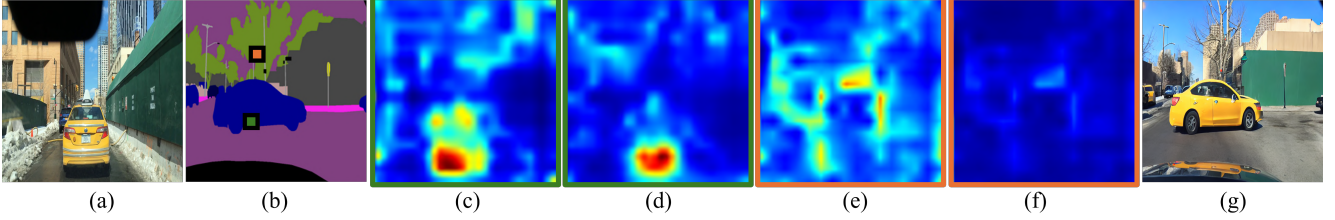


Figure 3. **Attention Visualization:** (a) Exemplar image with desired appearance, (b) target segmentation with desired structure, and (g) generated image. **Green** and **orange** markers in (b) indicate query points. (c) and (d) show the augmented self-attention map $Q_t^Y (K_t^X)^T$ from the green marker, before and after applying AM-Adapter, respectively. (e) and (f) show the augmented self-attention map $Q_t^Y (K_t^X)^T$ from the orange marker, before and after applying AM-Adapter, respectively. The green marker is within ‘car’ (present in the reference), while the orange marker is within ‘tree’ (absent in the reference). **AM-Adapter** refines mismatches in (c) and (e), demonstrating its effectiveness in (d) and (f).

ers. The cross-attention layers are guided by an additional text condition and the self-attention layer learns intra-relationships within the intermediate diffusion features. In the self-attention layer, the intermediate feature at each timestep t is projected into queries $Q_t \in \mathbb{R}^{h \times w \times d}$, keys $K_t \in \mathbb{R}^{h \times w \times d}$, and values $V_t \in \mathbb{R}^{h \times w \times d}$, where h , w , and d indicate height, width, and channels, respectively, and the attention score is calculated by matrix multiplication between Q_t and K_t . Then, V_t is warped to the queries based on the calculated attention score, formulated as:

$$\text{S-Att}(Q_t, K_t, V_t) = \text{Softmax}(A_t)V_t, \quad A_t = \frac{Q_t K_t^T}{\sqrt{d}}, \quad (1)$$

where $\text{S-Att}(\cdot)$ denotes the self-attention operation. $A_t \in \mathbb{R}^{h \times w \times h \times w}$ are attention scores. $\text{Softmax}(\cdot)$ normalizes the attention scores across the keys.

3.2. Problem Statement and Overview

Given an exemplar image $I^X \in \mathbb{R}^{H \times W \times 3}$ and a target segmentation map $S^Y \in \mathbb{R}^{H \times W \times 1}$, where H and W denote height and width, our goal is to generate a target image I^Y that retains the appearance of I^X , while maintaining the structure of S^Y . Prior works such as ControlNet [43], ControlNeXt [29], or related variants [15, 29, 44] commonly provide structural guidance through segmentation maps and adapt appearance using text control [43] or an additional image encoder [7, 41]. However, these methods fail to retain local details from I^X as they either do not take the exemplar image as input [29, 43] or compress local features into a global representation [7, 41].

To address this, we aim to enhance the local appearance from the exemplar image I^X in the synthesized target image I^Y , while retaining the target structure driven by S^Y . Our architecture consists of a dual-branch structure: an Appearance Net, denoted as $\epsilon_\theta^X(\cdot)$, and a Structure Net, denoted as $\epsilon_\theta^Y(\cdot)$. Specifically, I^X is passed through the VAE [31] to produce z_0^X in the latent space. z_0^X is then inverted into z_T^X by DDIM inversion [24]. z_T^X is subsequently reconstructed to z_0^X by the Appearance Net, guided by S^X . The Structure

Net synthesizes a target image \hat{I}^Y , starting from random Gaussian noise z_T^Y to z_0^Y guided by the target segmentation map S^Y . z_0^X and z_0^Y are decoded as \hat{I}^X and \hat{I}^Y , respectively, through the VAE [31]. At each time step, exemplar keys and values, K_t^X and V_t^X , from the Appearance Net are transferred to the augmented self-attention module in the Structure Net. Our appearance matching adapter (AM-Adapter) enhances the matching between Q_t^Y from Structure Net and K_t^X from Appearance Net, reflecting the semantic relationship between S^Y and S^X . The architecture is illustrated in Figure 4.

3.3. Baseline and Analysis

The most straightforward method to transfer exemplar’s appearance from Appearance Net into the Structure Net, as in previous works [2, 18, 26], could be to naively concatenate the exemplar’s keys K_t^X and values V_t^X with the corresponding target keys K_t^Y and values V_t^Y , which can formulate as:

$$\text{S-Att}(Q_t^Y, K_t^{\{Y,X\}}, V_t^{\{Y,X\}}) = \text{Softmax}(A_t^{\{Y,X\}})V_t^{\{Y,X\}}, \quad (2)$$

$$A_t^{\{Y,X\}} = \frac{Q_t^Y (K_t^{\{Y,X\}})^T}{\sqrt{d}}, \quad (3)$$

$$K_t^{\{Y,X\}} = \text{Concat}(K_t^Y, K_t^X), \quad (4)$$

$$V_t^{\{Y,X\}} = \text{Concat}(V_t^Y, V_t^X), \quad (5)$$

where $\text{Concat}(\cdot)$ indicates the concatenation operation. Here, we divide $A_t^{\{Y,X\}}$ into $A_t^{Y \rightarrow Y}$ and $A_t^{Y \rightarrow X}$, where $A_t^{Y \rightarrow Y}$ is the matching cost between Q_t^Y and K_t^Y , which learns the intra-relationships of the features in the synthesized image, while $A_t^{Y \rightarrow X}$ is the matching cost between the target queries Q_t^Y and the exemplar keys K_t^X , where the target queries Q_t^Y attend to the exemplar keys K_t^X and selectively integrate the corresponding exemplar values V_t^X . As discussed in [1], this process can be analyzed by transferring local appearance details in V_t^X into the target image based on the semantic matching between Q_t^Y and K_t^X .

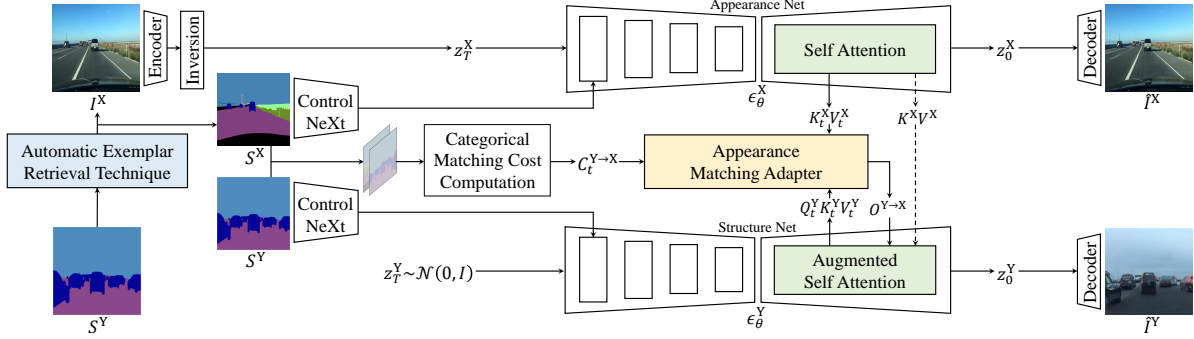


Figure 4. Overall Architecture.

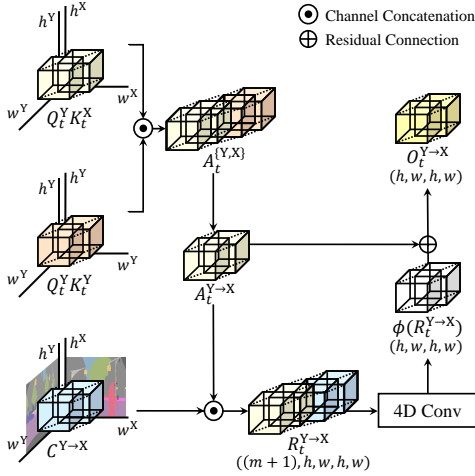


Figure 5. Appearance Matching Adapter.

However, as shown in Figure 9(c), this approach often produces suboptimal results, as it relies on implicit matching within the self-attention mechanism trained for generation, which can lead to inaccurate matches, particularly in complex domains (e.g., driving scenes). In particular, this results in mismatches across distinct categories (e.g., cars being matched to trees).

One solution to address this is to directly train the augmented self-attention module to enhance the implicit matching in the pre-trained diffusion model. However, as shown in Figure 9(d), this approach is challenging, as the model needs to learn both generation and matching at the same time, resulting in unstable training and overfitting.

3.4. Appearance Matching Adapter

To address this, we propose a learnable appearance matching adapter, AM-Adapter that enhances the implicit matching $A_t^{Y \rightarrow X}$ with semantic awareness in a data-driven manner. The detailed architecture is illustrated in Figure 5.

Categorical Matching Cost. To obtain improved matching, it is crucial to be aware of the categorical relationship between the exemplar and target images, as pixels in the same category serve as strong initial points for establish-

ing accurate correspondence. To this end, we first compute a categorical matching cost by calculating pixel-wise correspondences between the segmentation maps of the exemplar and target images, denoted by S^X and S^Y , respectively.

Given segmentation maps S^X and S^Y , which represent semantic labels, we build the binary categorical matching cost $C^{Y \rightarrow X}$ by identifying pixel positions in S^Y that match the categorical index of each pixel in S^X . This process is formulated as:

$$C^{Y \rightarrow X}(i, j, k, l) = \begin{cases} 1, & \text{if } S^Y(i, j) = S^X(k, l), \\ 0, & \text{otherwise,} \end{cases} \quad (6)$$

where $i, j \in [0, H) \times [0, W)$ and $k, l \in [0, H) \times [0, W)$.

Attention Aggregation Module. The most straightforward approach to apply the categorical matching cost $C^{Y \rightarrow X}$ is to directly multiply implicit matching cost $A_t^{Y \rightarrow X}$ by $C^{Y \rightarrow X}$ during the inference phase. However, as shown in Figure 9(e), while this method can filter out erroneous matches between different categories, it often fails to find the correct correspondences within the same category. This is because $C^{Y \rightarrow X}$ is a binary map that does not directly align with the attention scores in $A_t^{Y \rightarrow X}$ within the self-attention module.

To address this, inspired by prior works [10, 22], we propose a lightweight 4D convolution network to refine the implicit matching cost $A_t^{Y \rightarrow X}$ with the categorical matching cost $C^{Y \rightarrow X}$ in a data-driven manner, enabling more precise pixel-wise correspondence between exemplar and target. Note that, unlike 2D convolution networks, which process each image independently and do not capture local relationships between the exemplar and target, 4D convolution achieves reliable matching by identifying locally consistent regions across both images in 4D space.

Specifically, at each time step t , we concatenate the implicit matching cost $A_t^{Y \rightarrow X}$ and the categorical matching cost $C^{Y \rightarrow X}$ along the channel dimension. Here, to allow each self-attention head to learn distinct relationships, we retain the number of multiple heads, denoted as m , and thus $A_t^{Y \rightarrow X} \in \mathbb{R}^{h \times w \times h \times w \times (m+1)}$. This results in $R_t^{Y \rightarrow X} \in \mathbb{R}^{h \times w \times h \times w \times (m+1)}$, where h, w and $m+1$ repre-

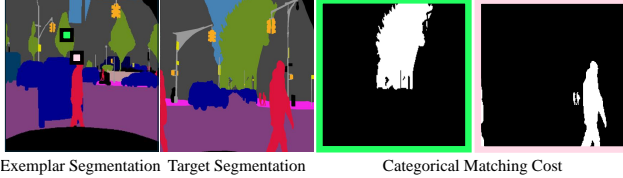


Figure 6. **Visualization of Categorical Matching Cost.** The green and pink markers denote the query points in the exemplar segmentation map. Our categorical matching cost effectively identifies binary categorical matches between the exemplar and target segmentation maps (best viewed in color).

sent the height, width and concatenated channel dimension, respectively. $C^{Y \rightarrow X}$ is downsampled to match the dimensions of $A_t^{Y \rightarrow X}$. The process is formulated as:

$$R_t^{Y \rightarrow X} = \text{Concat}(A_t^{Y \rightarrow X}, \text{Downsample}(C^{Y \rightarrow X})), \quad (7)$$

where Concat denotes concatenation operation along the channel dimension, while Downsample indicates the downsampling operation.

To enhance the matching cost with semantic awareness, the 4D convolution network aggregates the concatenated matching cost $R_t^{Y \rightarrow X}$ and outputs the refined matching cost. To stabilize the learning process, the refined cost is added to the original implicit matching cost $A_t^{Y \rightarrow X}$ through a residual connection, resulting in the final output $O_t^{Y \rightarrow X} \in \mathbb{R}^{h \times w \times h \times w}$. The overall process is formulated as:

$$O_t^{Y \rightarrow X} = \phi(R_t^{Y \rightarrow X}) + A_t^{Y \rightarrow X}, \quad (8)$$

Here, $\phi(\cdot)$ denotes the proposed learnable 4D convolution network. In Figure 3, we compare the attention maps from $A_t^{Y \rightarrow X}$ and $O_t^{Y \rightarrow X}$, highlighting the impact of our 4D cost aggregation module.

Finally, in the Structure Net, $A_t^{\{Y, X\}}$ at each time step t is enhanced by combining $O_t^{Y \rightarrow Y}$ and $A_t^{Y \rightarrow X}$.

3.5. Training

Exemplar-Target Pair. To train for local appearance transfer from the exemplar image to the target image, it is essential for both images to share similar local appearance. We achieve this through data augmentation techniques to create exemplar-target pairs with matching local appearance. Specifically, we apply different augmentations, such as random cropping [35] and flipping [45], to an anchor image to generate exemplar-target image pairs I^X and I_Y . The same augmentations are applied to the segmentation maps S^X and S^Y , producing corresponding augmented segmentation pairs. Using this paired dataset, we train the matching adapter to guide the pre-trained diffusion model in synthesizing the new target image that reflects the local appearance of the exemplar.

Stage-wise Training. The most direct approach to train our model is to jointly train ControlNeXt [29], the diffusion model, and our matching adapter. However, this poses

challenges in disentangling structural guidance from ControlNeXt, the generative capability of the diffusion model, and matching process from the adapter, leading to unstable training and potential overfitting, which degrades structural consistency, image quality, or matching performance. To mitigate this, we adopt a stage-wise training strategy: first, we train ControlNeXt with image-segmentation pairs, for fine-grained structural control. Next, to generate realistic samples in the desired domain, we train the diffusion model on the domain with ControlNeXt frozen. Finally, we train our matching adapter on the frozen Appearance Net and Structure Net, both of which use the same pre-trained diffusion model and ControlNeXt. The stage-wise approach effectively separates structural guidance, generation, and matching, achieving high performance in each component.

3.6. Inference

Retrieval-based Inference. During inference, previous tuning-free methods [1, 18] require manual selection of exemplar images. However, identifying suitable exemplars for generating content-rich images, such as driving scenes, is labor-intensive. To address this, we introduce an automatic exemplar retrieval technique. A basic approach selects the closest structural match from a pool of segmentation maps and uses the corresponding RGB image as the exemplar. However, we find that segmentation-based retrieval often misses finer structural details, resulting in suboptimal outcomes. To improve precision, we retrieve exemplar images based on structural similarity between RGB images. Specifically, we generate a random RGB image from the target segmentation map using Structure Net, preserving detailed structural information. We then convert this RGB image to grayscale, comparing it with grayscale images in the pool to find the most structurally similar exemplar. This process yields the top-1 exemplar RGB image for each target segmentation map. More details and ablation studies are available in Appendix C.2.

Matching Cost Guidance. To further enhance the matching between the exemplar and target, we propose a matching cost guidance technique during inference. Specifically, we apply classifier-free guidance [9] on the refined matching cost $O_t^{Y \rightarrow X}$, which is formulated as:

$$\tilde{\epsilon}(z_t^Y) = \epsilon_\theta(z_t^Y) + (1 + s) (\epsilon_\theta(z_t^Y, O_t^{Y \rightarrow X}) - \epsilon_\theta(z_t^Y)). \quad (9)$$

Here, s is the guidance scale.

4. Experiments

4.1. Experimental Settings

Dataset. Since there is no established benchmark for semantic image synthesis, we created a dedicated dataset featuring complex driving scenes with diverse structure-appearance pairs. Our dataset comprises 300 pairs col-



Figure 7. **Qualitative Comparison on BDD100K [42] and Cityscapes [4]:** Compared to previous methods [1, 18, 23, 41, 43] that fail to transfer local appearance or find accurate matching, AM-Adapter effectively achieves precise matching in content-rich, complex scenes.

Methods	Training	BDD100K [42]			Cityscapes [4]		
		Self-sim. (\downarrow)	I_{CLIP} (\uparrow)	FID (\downarrow)	Self-sim. (\downarrow)	I_{CLIP} (\uparrow)	FID (\downarrow)
ControlNet [43]	✓	0.052	0.638	95.10	0.058	0.761	113.87
ControlNeXt [29]	✓	0.047	0.731	94.48	0.055	0.760	130.04
FreeControl [23]	✗	0.062	0.575	179.00	0.073	0.690	211.28
Cross-Image Attention [1]	✗	0.177	0.643	233.76	0.133	0.754	214.31
Ctrl-X [18]	✗	0.051	0.700	107.06	0.058	0.818	112.49
ControlNet [43] + IP-Adapter [41]	✓	0.049	0.805	84.82	0.049	0.823	115.98
AM-Adapter (Ours)	✓	0.041	0.819	75.89	0.048	0.835	85.67

Table 1. Quantitative Comparison.

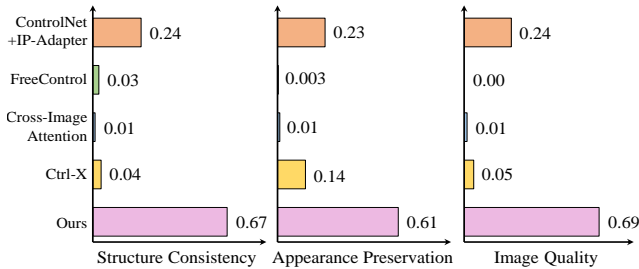


Figure 8. User Study.

lected from two widely used datasets: BDD100K [42] and Cityscapes [4]. Further details are provided in Appendix B.1.

Evaluation Metric. Following previous studies [1, 18, 26, 38], we evaluate our method using widely adopted metrics for (1) structural consistency, (2) appearance preservation, and (3) image quality. To assess structural consistency between the generated image and the given segmentation map, We use the self-similarity metric, denoted as Self-Sim (\downarrow) [37]. To evaluate appearance preservation, we compute the CLIP image similarity denoted as I_{CLIP} (\uparrow) [32] between the generated image and the exemplar image. To assess image quality, we calculate FID (\downarrow) [5]. Additional details about the evaluation metrics are provided in Appendix B.2.

User Study. We conducted a user study comparing our model to previous works [1, 18, 23, 41, 43]. 45 participants evaluated the generated images based on structure preservation, appearance preservation and image quality. Additional details on the user study are in Appendix B.3.

4.2. Comparison

Figure 7 and Table 1 present qualitative and quantitative comparisons with other models [1, 18, 23, 41, 43]. ControlNet [43] + IP-Adapter [41] achieves high structure preservation (Self-Sim), however, since IP-Adapter captures only global exemplar appearance, it often fails to preserve detailed appearance from the exemplar (I_{CLIP}). Pre-

vious hand-crafted attention control methods [1, 18, 23] show suboptimal matching performance (I_{CLIP}), leading to blurry and distorted outputs (FID) or disregarding structural guidance from target segmentation maps (Self-Sim.). In contrast, our AM-Adapter surpasses prior efforts in structural consistency (Self-Sim), appearance preservation (I_{CLIP}), and image quality (FID), demonstrating its effectiveness in preserving local details from the exemplar while closely reflecting the target structure. Figure 8 further demonstrates that our method consistently surpasses prior works in appearance preservation, structural consistency, and image quality. Additional results and applications are provided in Appendix C.1 and Appendix D.

4.3. Ablation Study

In Figure 9 and Table 2, we demonstrate the effectiveness of each component in our model. We conduct a comprehensive analysis of our model components from the following perspectives: (1) the selection of the model baseline, exploring different strategies including key-value replacement (MasaCtrl [2]), warping with diffusion features (DreamMatcher [26]) and augmentation (Augmented Self-Attention); (2) the effect of fine-tuning on the baseline, analyzing the performance of Augmented Self-Attention and Augmented Self-Attention with fine-tuning; and (3) the effectiveness of incorporating a learnable cost, achieved through our proposed AM-Adapter, in contrast to using a Categorical Matching Cost.

(I) shows the results of ControlNeXt [29] without an input exemplar. (a) and (II) represent the results of MasaCtrl [2], which replaces the key and value of the synthesized target image with those of the exemplar image. While this achieves strong appearance fidelity, it severely disrupts semantic alignment, resulting in structurally incoherent outputs. (b) and (III) show the results of DreamMatcher [26], which enhances implicit matching by leveraging diffusion features. However, its implicit matching struggles in complex scenes, leading to less accurate appearance transfer. (c) and (IV) present the results of augmented self-attention

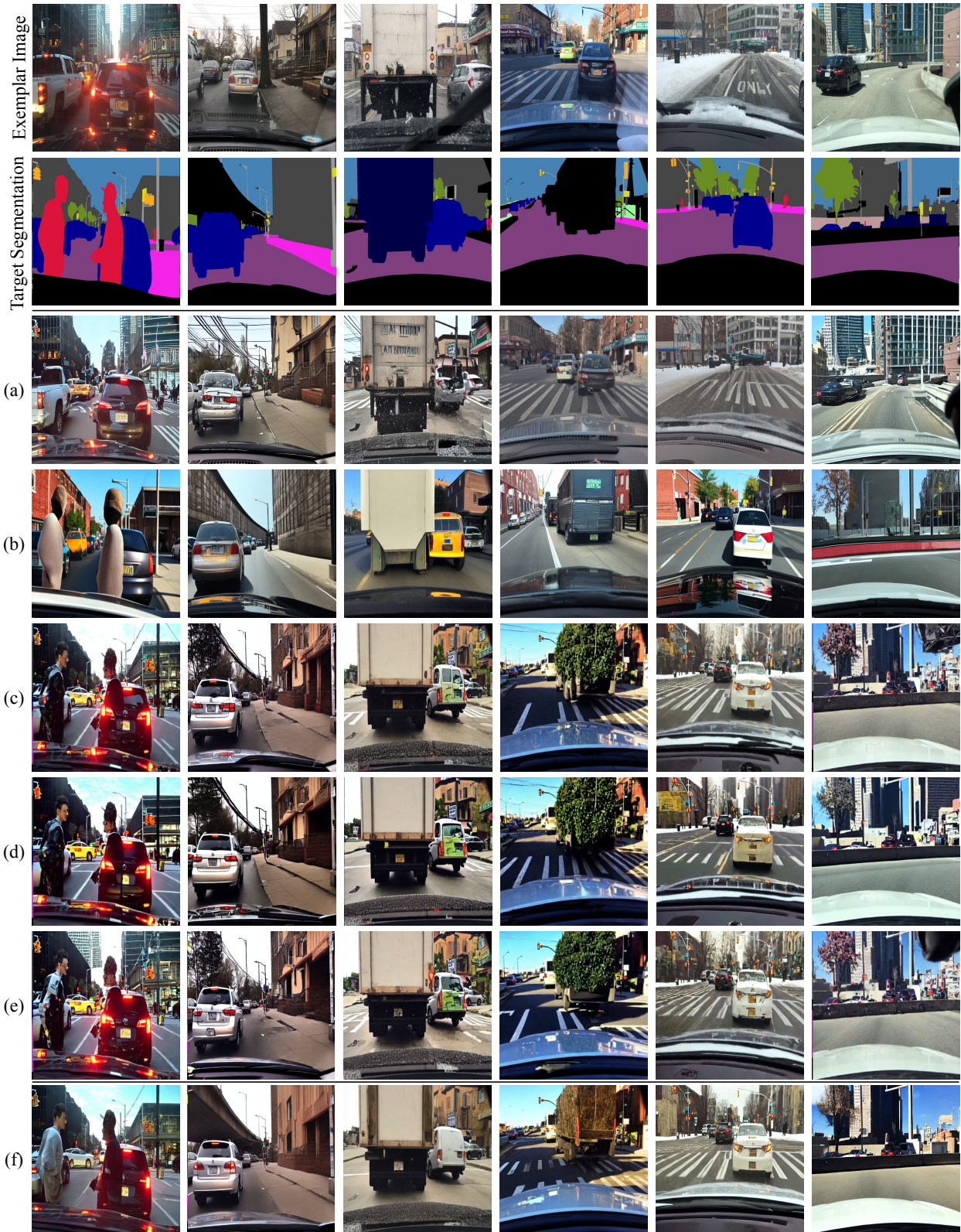


Figure 9. **Ablation Study on BDD100K [42] Dataset:** Given pretrained structure-guidance and generation models in our framework, (a) key-value replacement (MasaCtrl [2]), (b) DreamMatcher [26], (c) augmented self-attention, (d) augmented self-attention w/ finetuning, (e) augmented self-attention combined with categorical matching cost through multiplication, and (f) **AM-Adapter (Ours)**. Our final method achieves the optimal results.

	Methods	BDD100K [42]			Cityscapes [4]		
		Self-Sim. (\downarrow)	I_{CLIP} (\uparrow)	FID (\downarrow)	Self-Sim. (\downarrow)	I_{CLIP} (\uparrow)	FID (\downarrow)
	Exemplar image	0.052	1.000	44.23	0.049	1.000	40.00
(I)	Pre-training (ControlNeXt [29])	0.047	0.731	94.48	0.055	0.760	130.04
(II)	(I) + MasaCtrl [2]	0.047	0.872	79.45	0.052	0.885	81.37
(III)	(I) + DreamMatcher [26]	0.046	0.724	79.34	0.061	0.776	97.93
(IV)	(I) + Augmented Self-Attention	0.043	0.815	78.13	0.048	0.830	115.89
(V)	(IV) + w/ Fine-tuning	0.043	0.808	77.75	0.051	0.810	134.00
(VI)	(IV) + Categorical Matching Cost	0.043	0.817	76.76	0.050	0.832	96.36
(VII)	AM-Adapter (Ours)	0.041	0.819	75.89	0.048	0.835	85.67

Table 2. **Ablation Study.** Although the table displays scores rounded to three decimal places, we determine the rankings based on precision to the fourth decimal place.

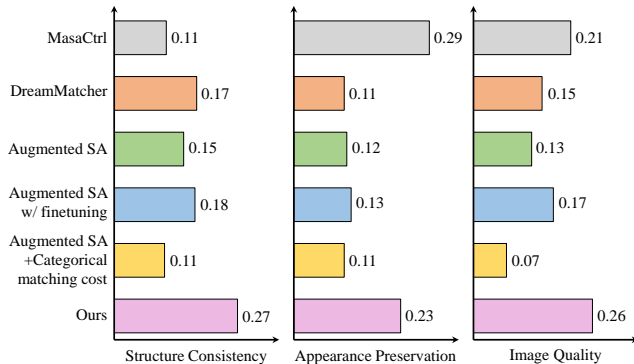


Figure 10. **User Study on Ablation Study.**

without fine-tuning. Unlike (I), (c) and (IV) incorporate appearance, leading to a substantial improvement in appearance preservation. However, due to its reliance on implicit matching, it fails to correct mismatches (e.g., car matched to pedestrian, trees matched to truck, bridge matched to trees), resulting in distorted outputs. In comparison, (d) and (V) show the results of a fine-tuned network employing augmented self-attention. While learning both matching and generation simultaneously, the unstable learning signal causes mismatched correspondences to remain unresolved and amplified during generation. To enhance matching, (e) and (VI) represent the results of simply multiplying the augmented self-attention module by the categorical matching cost. Compared to (c) and (e), it demonstrates improved ability to correct mismatches, but its matching performance remains limited, resulting in suboptimal, distorted outputs. In contrast, AM-Adapter (f) and (VII) effectively disentangle matching from generation, maximizing the capabilities of both. This approach significantly improves overall image quality and instance-level details while demonstrating superior matching performance, as evident in transferred visual attributes such as vehicle color, and building structures.

Additional results and further analyses are provided in the Appendix C.2.

User Study. Figure 10 summarizes a human evaluation study on different configurations of the AM-Adapter, based on the criteria of structural consistency, appearance preservation, and image quality. A total of 33 participants each responded to 24 questions. For a fair comparison, we sampled generated images from a large pool, using the same exemplar-target segmentation pairs for different components. Additional details are presented in Appendix B.3

5. Conclusion

We introduce the Appearance Matching Adapter (AM-Adapter), a learnable framework designed to enhance local appearance transfer by combining implicit matching costs from self-attention with categorical matching costs derived from segmentation maps. Our approach effectively preserves spatial structure while ensuring precise semantic correspondence. To disentangle structural guidance, generation, and matching processes, we employ a stage-wise training strategy. Furthermore, during inference, we propose a retrieval technique that optimizes matchable regions. Extensive experiments demonstrate the effectiveness of our method, highlighting its robustness in challenging scenarios such as driving scenes, and its applications such as image-to-image translation and segmentation-based image editing.

References

- [1] Yuval Alaluf, Daniel Garibi, Or Patashnik, Hadar Averbuch-Elor, and Daniel Cohen-Or. Cross-image attention for zero-shot appearance transfer. In *ACM SIGGRAPH 2024 Conference Papers*, pages 1–12, 2024. 2, 3, 4, 6, 7, 8, 13, 14, 18, 20
- [2] Mingdeng Cao, Xintao Wang, Zhongang Qi, Ying Shan, Xiaohu Qie, and Yinqiang Zheng. Masactrl: Tuning-free mutual self-attention control for consistent image synthesis and editing. In *Proceedings of the IEEE/CVF International Conference on Computer Vision*, pages 22560–22570, 2023. 2, 4, 8, 9, 10, 14, 18
- [3] Dimitrios Christodoulou and Mads Kuhlmann-Jørgensen. Finding the subjective truth: Collecting 2 million votes for comprehensive gen-ai model evaluation. *arXiv preprint arXiv:2409.11904*, 2024. 13
- [4] Marius Cordts, Mohamed Omran, Sebastian Ramos, Timo Rehfeld, Markus Enzweiler, Rodrigo Benenson, Uwe Franke, Stefan Roth, and Bernt Schiele. The cityscapes dataset for semantic urban scene understanding. In *Proceedings of the IEEE conference on computer vision and pattern recognition*, pages 3213–3223, 2016. 3, 7, 8, 10, 13
- [5] Prafulla Dhariwal and Alex Nichol. Diffusion models beat gans on image synthesis, 2021. 8, 13
- [6] George Eskandar, Diandian Guo, Karim Guirguis, and Bin Yang. Towards pragmatic semantic image synthesis for urban scenes, 2023. 2
- [7] Rinon Gal, Moab Arar, Yuval Atzmon, Amit H Bermano, Gal Chechik, and Daniel Cohen-Or. Encoder-based domain tuning for fast personalization of text-to-image models. *ACM Transactions on Graphics (TOG)*, 42(4):1–13, 2023. 2, 3, 4, 13
- [8] Tewodros Habtegebrail, Varun Jampani, Orazio Gallo, and Didier Stricker. Generative view synthesis: From single-view semantics to novel-view images, 2020. 2
- [9] Jonathan Ho and Tim Salimans. Classifier-free diffusion guidance, 2022. 6, 15
- [10] Sunghwan Hong, Jisu Nam, Seokju Cho, Susung Hong, Sangryul Jeon, Dongbo Min, and Seungryong Kim. Neural matching fields: Implicit representation of matching fields for visual correspondence, 2022. 5
- [11] Li Hu. Animate anyone: Consistent and controllable image-to-video synthesis for character animation. In *Proceedings of the IEEE/CVF Conference on Computer Vision and Pattern Recognition*, pages 8153–8163, 2024. 2
- [12] Li Hu, Xin Gao, Peng Zhang, Ke Sun, Bang Zhang, and Liefeng Bo. Animate anyone: Consistent and controllable image-to-video synthesis for character animation, 2024. 2
- [13] Dongfu Jiang, Max Ku, Tianle Li, Yuansheng Ni, Shizhuo Sun, Rongqi Fan, and Wenhui Chen. Genai arena: An open evaluation platform for generative models. *arXiv preprint arXiv:2406.04485*, 2024. 13
- [14] Baiqi Li, Zhiqiu Lin, Deepak Pathak, Jiayao Li, Yixin Fei, Kewen Wu, Tiffany Ling, Xide Xia, Pengchuan Zhang, Graham Neubig, et al. Genai-bench: Evaluating and improving compositional text-to-visual generation. *arXiv preprint arXiv:2406.13743*, 2024. 13
- [15] Ming Li, Taojiannan Yang, Huafeng Kuang, Jie Wu, Zhaoning Wang, Xuefeng Xiao, and Chen Chen. Controlnet++: Improving conditional controls with efficient consistency feedback. In *European Conference on Computer Vision*, pages 129–147. Springer, 2025. 2, 3, 4, 13
- [16] Yuheng Li, Haotian Liu, Qingyang Wu, Fangzhou Mu, Jianwei Yang, Jianfeng Gao, Chunyuan Li, and Yong Jae Lee. Gligen: Open-set grounded text-to-image generation. In *Proceedings of the IEEE/CVF Conference on Computer Vision and Pattern Recognition*, pages 22511–22521, 2023. 2, 3, 13
- [17] Zhen Li, Mingdeng Cao, Xintao Wang, Zhongang Qi, Ming-Ming Cheng, and Ying Shan. Photomaker: Customizing realistic human photos via stacked id embedding. In *Proceedings of the IEEE/CVF Conference on Computer Vision and Pattern Recognition*, pages 8640–8650, 2024. 2, 3, 13
- [18] Kuan Heng Lin, Sicheng Mo, Ben Klingher, Fangzhou Mu, and Bolei Zhou. Ctrl-x: Controlling structure and appearance for text-to-image generation without guidance. *arXiv preprint arXiv:2406.07540*, 2024. 2, 3, 4, 6, 7, 8, 13, 14, 18, 20
- [19] Zhiqiu Lin, Deepak Pathak, Baiqi Li, Jiayao Li, Xide Xia, Graham Neubig, Pengchuan Zhang, and Deva Ramanan. Evaluating text-to-visual generation with image-to-text generation. In *European Conference on Computer Vision*, pages 366–384. Springer, 2025. 13
- [20] Ilya Loshchilov and Frank Hutter. Decoupled weight decay regularization, 2019. 13
- [21] Wuyang Luo, Su Yang, Xinjian Zhang, and Weishan Zhang. Siedob: Semantic image editing by disentangling object and background, 2023. 16
- [22] Juhong Min, Dahyun Kang, and Minsu Cho. Hypercorrelation squeeze for few-shot segmentation, 2021. 5
- [23] Sicheng Mo, Fangzhou Mu, Kuan Heng Lin, Yanli Liu, Bochen Guan, Yin Li, and Bolei Zhou. Freecontrol: Training-free spatial control of any text-to-image diffusion model with any condition. In *Proceedings of the IEEE/CVF Conference on Computer Vision and Pattern Recognition*, pages 7465–7475, 2024. 7, 8, 13, 14, 18, 20
- [24] Ron Mokady, Amir Hertz, Kfir Aberman, Yael Pritch, and Daniel Cohen-Or. Null-text inversion for editing real images using guided diffusion models. In *Proceedings of the IEEE/CVF Conference on Computer Vision and Pattern Recognition*, pages 6038–6047, 2023. 4
- [25] Chong Mou, Xintao Wang, Liangbin Xie, Yanze Wu, Jian Zhang, Zhongang Qi, and Ying Shan. T2i-adapter: Learning adapters to dig out more controllable ability for text-to-image diffusion models. In *Proceedings of the AAAI Conference on Artificial Intelligence*, pages 4296–4304, 2024. 2, 3, 13
- [26] Jisu Nam, Heesu Kim, DongJae Lee, Siyoon Jin, Seungryong Kim, and Seunggyu Chang. Dreammatcher: Appearance matching self-attention for semantically-consistent text-to-image personalization. In *Proceedings of the IEEE/CVF Conference on Computer Vision and Pattern Recognition*, pages 8100–8110, 2024. 2, 3, 4, 8, 9, 10, 13, 14, 18
- [27] Taesung Park, Ming-Yu Liu, Ting-Chun Wang, and Jun-Yan Zhu. Semantic image synthesis with spatially-adaptive normalization. In *Proceedings of the IEEE/CVF conference on*

- computer vision and pattern recognition*, pages 2337–2346, 2019. [2](#), [3](#), [13](#)
- [28] Gaurav Parmar, Taesung Park, Srinivasa Narasimhan, and Jun-Yan Zhu. One-step image translation with text-to-image models, 2024. [13](#)
- [29] Bohao Peng, Jian Wang, Yuechen Zhang, Wenbo Li, Ming-Chang Yang, and Jiaya Jia. Controlnext: Powerful and efficient control for image and video generation. *arXiv preprint arXiv:2408.06070*, 2024. [2](#), [3](#), [4](#), [6](#), [8](#), [10](#), [13](#), [17](#)
- [30] Xu Peng, Junwei Zhu, Boyuan Jiang, Ying Tai, Donghao Luo, Jiangning Zhang, Wei Lin, Taisong Jin, Chengjie Wang, and Rongrong Ji. Portraitbooth: A versatile portrait model for fast identity-preserved personalization. In *Proceedings of the IEEE/CVF Conference on Computer Vision and Pattern Recognition*, pages 27080–27090, 2024. [2](#), [3](#), [13](#)
- [31] Yunchen Pu, Zhe Gan, Ricardo Henao, Xin Yuan, Chunyuan Li, Andrew Stevens, and Lawrence Carin. Variational autoencoder for deep learning of images, labels and captions. *Advances in neural information processing systems*, 29, 2016. [4](#)
- [32] Alec Radford, Jong Wook Kim, Chris Hallacy, Aditya Ramesh, Gabriel Goh, Sandhini Agarwal, Girish Sastry, Amanda Askell, Pamela Mishkin, Jack Clark, Gretchen Krueger, and Ilya Sutskever. Learning transferable visual models from natural language supervision, 2021. [2](#), [3](#), [8](#), [13](#)
- [33] Robin Rombach, Andreas Blattmann, Dominik Lorenz, Patrick Esser, and Björn Ommer. High-resolution image synthesis with latent diffusion models. In *Proceedings of the IEEE/CVF conference on computer vision and pattern recognition*, pages 10684–10695, 2022. [3](#)
- [34] Jiaming Song, Chenlin Meng, and Stefano Ermon. Denoising diffusion implicit models. *arXiv preprint arXiv:2010.02502*, 2020. [13](#)
- [35] Ryo Takahashi, Takashi Matsubara, and Kuniaki Uehara. Data augmentation using random image cropping and patching for deep cnns. *IEEE Transactions on Circuits and Systems for Video Technology*, 30(9):2917–2931, 2020. [6](#)
- [36] Zhiyu Tan, Xiaomeng Yang, Luo Zheng Qin, Mengping Yang, Cheng Zhang, and Hao Li. Evalalign: Evaluating text-to-image models through precision alignment of multimodal large models with supervised fine-tuning to human annotations. *arXiv preprint arXiv:2406.16562*, 2024. [13](#)
- [37] Narek Tumanyan, Omer Bar-Tal, Shai Bagon, and Tali Dekel. Splicing vit features for semantic appearance transfer, 2022. [8](#), [13](#), [14](#)
- [38] Weilun Wang, Jianmin Bao, Wengang Zhou, Dongdong Chen, Dong Chen, Lu Yuan, and Houqiang Li. Semantic image synthesis via diffusion models. *arXiv preprint arXiv:2207.00050*, 2022. [2](#), [3](#), [8](#), [13](#)
- [39] Guangxuan Xiao, Tianwei Yin, William T Freeman, Frédo Durand, and Song Han. Fastcomposer: Tuning-free multi-subject image generation with localized attention. *International Journal of Computer Vision*, pages 1–20, 2024. [2](#), [3](#), [13](#)
- [40] Han Xue, Zhiwu Huang, Qianru Sun, Li Song, and Wenjun Zhang. Freestyle layout-to-image synthesis. In *Proceedings of the IEEE/CVF Conference on Computer Vision and Pattern Recognition*, pages 14256–14266, 2023. [2](#)
- [41] Hu Ye, Jun Zhang, Sibio Liu, Xiao Han, and Wei Yang. Ip-adapter: Text compatible image prompt adapter for text-to-image diffusion models. *arXiv preprint arXiv:2308.06721*, 2023. [2](#), [3](#), [4](#), [7](#), [8](#), [13](#), [14](#), [18](#), [20](#)
- [42] Fisher Yu, Haofeng Chen, Xin Wang, Wenqi Xian, Yingying Chen, Fangchen Liu, Vashisht Madhavan, and Trevor Darrell. Bdd100k: A diverse driving dataset for heterogeneous multitask learning. In *Proceedings of the IEEE/CVF conference on computer vision and pattern recognition*, pages 2636–2645, 2020. [3](#), [7](#), [8](#), [9](#), [10](#), [13](#), [16](#), [20](#), [23](#)
- [43] Lvmin Zhang, Anyi Rao, and Maneesh Agrawala. Adding conditional control to text-to-image diffusion models. In *Proceedings of the IEEE/CVF International Conference on Computer Vision*, pages 3836–3847, 2023. [2](#), [3](#), [4](#), [7](#), [8](#), [13](#), [14](#), [18](#), [20](#)
- [44] Shihao Zhao, Dongdong Chen, Yen-Chun Chen, Jianmin Bao, Shaozhe Hao, Lu Yuan, and Kwan-Yee K Wong. Uni-controlnet: All-in-one control to text-to-image diffusion models. *Advances in Neural Information Processing Systems*, 36, 2024. [2](#), [3](#), [4](#), [13](#)
- [45] Jing Zhou, Yanan Zheng, Jie Tang, Jian Li, and Zhilin Yang. Flipda: Effective and robust data augmentation for few-shot learning, 2022. [6](#)
- [46] Yan Zhuang, Benjamin Hou, Tejas Sudharshan Mathai, Pritam Mukherjee, Boah Kim, and Ronald M. Summers. Semantic image synthesis for abdominal ct, 2023. [2](#)

Appearance Matching Adapter for Exemplar-based Semantic Image Synthesis

Supplementary Material

In this material, Section A describes the implementation details of our experiments, while Section B elaborates the details of the evaluation process. Section C presents additional results, including qualitative, quantitative analyses and user studies. Finally, in Section D, we demonstrate the versatility of our work through various applications. Section E discusses the limitations of our work and provides a broader discussion.

A. Implementation Details

For all experiment, we used a single NVIDIA A6000 GPU. For training, we utilized 7K exemplar-target segmentation pairs from the BDD100K [42] dataset. During the first stage training, ControlNeXt [29] was trained with a batch size of 2 and a resolution of 512, using a learning rate of $1e - 5$, and the training process lasted approximately 9 hours. In the second stage, AM-Adapter was trained with a batch size of 1 and a resolution of 512 for 25,000 steps, taking around 14 hours. We used the same learning rate $1e - 5$, with the AdamW [20] optimizer applied in both stages. We utilized the DDIM [34] sampler for both inversion and sampling, with the number of timesteps T set to 20. The Augmented Self-Attention is applied across all self-attention layers of the UNet, denoted as $L \in [0, 9]$, while the AM-Adapter is applied to all self-attention layers except for the first block of the encoder, represented as $L \in [1, 9]$. This approach avoids the structural conflict and prevents interference between the two effects, as the cross-normalized features from ControlNeXt [29] are added after the first downsampling block. We set the guidance scale to $s = 7.5$ for both text and matching guidance.

B. Evaluation

B.1. Dataset

Prior works in Semantic Image Synthesis [15, 16, 25, 27, 29, 38, 43, 44] and Exemplar-based Semantic Image Synthesis [7, 17, 30, 39, 41] have used different datasets for evaluation. Commonly, prior methods [18] assemble image dataset from the web and hand annotated the condition such as segmentation, sketch or edge drawing. Since no established benchmark exists for Exemplar-based Semantic Image Synthesis, we constructed an evaluation dataset tailored to our task, featuring complex driving scenes with diverse structure-appearance pairs. Specifically, we evaluated our method on two commonly used driving scene datasets: BDD100K [42] and Cityscapes [4]. For evaluation, we randomly selected 300 segmentation maps each

from BDD100K and Cityscapes, resulting in a total of 600 segmentation maps.

Our goal is to achieve semantic-aware local appearance transfer in complex scenarios. As part of this effort, we propose a retrieval technique that automatically selects exemplars while maximizing matchable regions, as discussed in Section 3.6 of the main paper. Therefore, the exemplar segmentation-image pairs in our evaluation dataset consist of two types: 300 pairs retrieved using 300 target segmentation maps and 300 pairs randomly selected.

B.2. Evaluation Metrics

For quantitative evaluation, we categorized our analysis into three perspectives: structure consistency, appearance preservation and image quality. Following previous studies [18, 28], we adopted Self-Sim. [37] metrics to evaluate structure consistency. To evaluate appearance preservation, following prior works [26], we computed CLIP image similarity [32], denoted as I_{CLIP} . For image quality assessment, we measured FID [5]. Table 1 of the main paper presents the results for the three metrics.

While our AM-Adapter outperforms other methods across all metrics, as noted in [3, 13, 14, 19, 36], we emphasize that these metrics do not fully align with human preferences. This is because they extract either global features or small local features from the generated images and conditions (segmentation maps and exemplar RGB images) and calculate distances between these features. To address this limitation, we conducted the user study for a more reliable evaluation.

B.3. User Study Details

Figure 13 presents an example question from the user study. We conducted a human evaluation study comparing AM-Adapter and previous works [1, 18, 23, 41, 43] in terms of structure consistency, appearance preservation, and image quality. For structure consistency, we provided the target segmentation map and the generated images from different methods, and users were asked to select which method better represents the semantic structure in the target segmentation map. For appearance preservation, we provided the exemplar image and the generated images from different methods, and participants were asked to choose which generated image better captures the appearance in the exemplar. Lastly, participants were shown only the generated images and asked to select the one that achieved the highest image quality. A total of 45 participants responded to 18 questions. For a fair comparison, we sampled generated images from a large pool sharing the same exemplar image

for three different methods to ensure intra-rater reliability. Figure 8 in the main paper summarizes the results, showing that our model outperforms others across all three criteria.

Figure 14 shows an example question from the user study comparing AM-Adapter with its individual components. The evaluation was conducted using the same criteria of structure preservation, appearance preservation and image quality to assess the role of each component in the overall performance. A total of 33 participants responded to 24 questions. For a fair comparison, generated images were samples from a shared pool associated with the same exemplar image and same target segmentation map across all methods. The results, summarized in Figure 10 in the main paper, show that AM-Adapter achieves a balanced and consistently high performance across all three criteria.

C. Additional Results

C.1. Qualitative Results

Figure 15 shows additional qualitative results of AM-Adapter. We present more qualitative results comparing our method with others, including ControlNet [43] + IP-Adapter [41], FreeControl [23], Cross-Image Attention [1], and Ctrl-X [18], in Figure 16, which further demonstrates the effectiveness of our method.

C.2. Ablation Study

Figure 9, Figure 11, Table 2 and Table 3 summarize the following ablation study.

MasaCtrl vs. DreamMatcher vs. Augmented Self-Attention. As shown in Figure 9 and Table 2, we conducted a comparative analysis of the Augmented Self-Attention against two representative hand-crafted attention control methods, MasaCtrl [2] and DreamMatcher [26], which focus on implicit matching within self-attention mechanisms. MasaCtrl replaces the key and value of the synthesized target image with those of the exemplar image, while DreamMatcher enhances implicit matching by leveraging diffusion features for improved correspondence.

MasaCtrl heavily relies on implicit matching in the self-attention module, often resulting in inaccurate appearance transfers to semantically misaligned regions, thereby disrupting the target structure that aligns with the structural conditions. Furthermore, key-value replacement cannot generate new elements that are absent in the exemplar, as it discards the original keys and values from the target and replaces them with those from the exemplar. This limitation causes key-value replacement (MasaCtrl) to exhibit high I_{CLIP} , as it discards the original key-value pairs of the target and copies and pastes the exemplar’s appearance into the target image based on incorrect matching. This is further demonstrated by the Self-Sim. [37] of MasaCtrl in Table 2 and the structural consistency results from the user

study 10, which show that key-value replacement disrupts the structural consistency between generated images and the given semantic conditions. Notably, the metric of exemplar image in Table 2 reflects cases where the same appearance exemplar is used, which naturally leads to very high I_{CLIP} scores due to the identical appearance. Similarly, MasaCtrl achieves high scores even when matching fails, as it transfers all appearance information from the exemplar to the target.

In contrast, as demonstrated in Figure 9 and Table 2, DreamMatcher better preserves the target structure by leveraging improved semantic matching and using intermediate diffusion features to align the exemplar’s appearance with the target image. However, its appearance preservation is highly dependent on the exemplar image, as relying solely on hand-crafted matching with diffusion features is insufficient for establishing accurate correspondence in content-rich images, such as driving scenes, which require precise matching.

As a result, to achieve our goal of accurate transfer in complex scenes, we adopt Augmented Self-Attention as our baseline, which is outlined in Section 3.3 of the main paper. As shown in Figure 9 and Table 2, Augmented Self-Attention selectively incorporates keys and values from both the exemplar and the target, effectively preserving the desired target structure while transferring the exemplar’s local appearance. Due to this selectivity, I_{CLIP} is lower compared to key-value replacement, which indiscriminately transfers the entire appearance information from the exemplar. However, Augmented Self-Attention demonstrates a superior human evaluation score compared to MasaCtrl [2] and DreamMatcher [26], indicating that it concurrently achieves appearance transfer and structural consistency.

Impact of Fine-tuning. Nevertheless, as discussed in Section 3.3 in the main paper, relying solely on the implicit matching of the Augmented Self-Attention still leads to the mismatches. The most straightforward approach to address this issue is fine-tuning the model. However, as shown in Figure 9 (c) and (d) and discussed in Section 4.3, it is shown that fine-tuning degrades detailed appearance preservation, as it requires learning both generation and matching simultaneously, which leads to unstable training and overfitting. This is further demonstrated in the (V) in Table 2, (d) in Figure 9.

Categorical Matching Cost vs. Learnable Matching Cost (AM-Adapter). To concurrently achieve matching and generation, we refine the implicit matching with semantic awareness using segmentation maps in a data-driven manner, rather than fine-tuning the entire model. In Section 3.4 of the main paper, we compare categorical matching cost with AM-Adapter. (e) and (f) in Figure 9 further demonstrate the effectiveness of AM-Adapter compared to

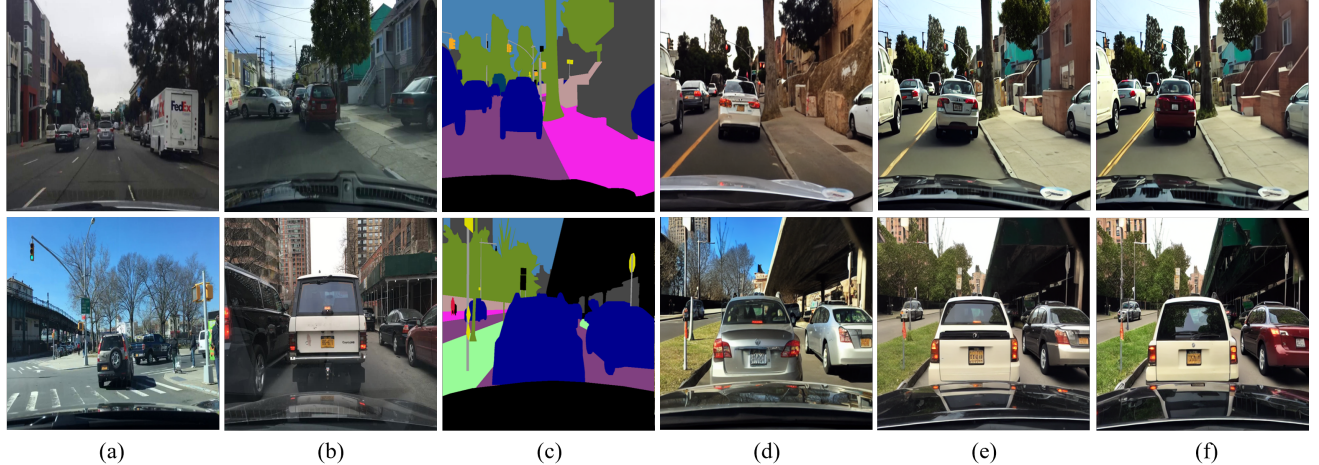


Figure 11. **Ablation on Inference:** (a) random exemplar image, (b) retrieved exemplar image, (c) target segmentation map with desired structure, results generated (d) without retrieval or matching guidance, (e) with retrieval but without matching guidance, and (f) with both retrieval and matching guidance.

categorical matching cost.

Inference. Figure 11 and Table 3 illustrate the effects of our proposed retrieval technique and matching guidance during inference. (a) represents a randomly selected exemplar image, and (b) represents a retrieved exemplar image. (c) and (I) display the results when a random exemplar image is used as input without retrieval. In contrast, (d) and (II) utilize an exemplar image that is structurally most similar to the target condition, resulting in higher appearance preservation compared to (a). Notably, this retrieval-based approach results in a significant increase in I_{CLIP} scores, increasing the matchable regions and transferring more appearance information from the exemplar. Finally, (e) and (III) show the results of applying matching guidance using classifier-free guidance [9], highlighting the effectiveness of matching guidance in achieving accurate results. Figure 17 presents the detailed mechanism of how the retrieval process operates and Figure 18 illustrates retrieved exemplar images from target segmentation maps obtained by our retrieval technique.

C.3. Additional Analysis

Figure 12 presents the additional examples of attention visualizations before and after applying the AM-Adapter, further highlighting the effectiveness of our model. The green markers indicate objects that are absent in the exemplar, while the orange markers denote objects that are present in the exemplar.

For instance, in the first row, the green marker highlights a query point corresponding to a ‘building’ that is absent in the exemplar. After applying the AM-Adapter, the attention associated with unrelated regions is significantly suppressed. The orange marker, on the other hand, indicates a query point on the top of a ‘trailer’. After applying AM-

	Component	Self-Sim. ↓	I_{CLIP} ↑	FID ↓
(I)	AM-Adapter	0.043	0.741	79.05
(II)	(I) + Retrieval	<u>0.041</u>	<u>0.814</u>	<u>77.15</u>
(III)	(II) + Matching Guidance (Ours)	0.041	0.819	75.89

Table 3. **Ablation Study on Inference.**

Adapter, the attention becomes more localized, concentrating more effectively on the relevant regions. In the second row, the green marker represents a query point corresponding to a ‘truck’ that does not appear in the exemplar. After the AM-Adapter is applied, mismatches in the attention are reduced, further aligning the attention with the target structure. Similarly, the orange marker identifies a query point near the right rear light of a ‘vehicle’. With the adapter applied, the attention becomes more localized, exhibiting enhanced focus on the intended area.

D. Applications

D.1. Segmentation-Guided Image Editing

Figure 19 and Figure 20 illustrate the results of AM-Adapter to segmentation-based editing applications, specifically object removal and addition, respectively. These results showcase the versatility of AM-Adapter in generating high-quality images while adhering to modified semantic structures.

In Figure 19, we demonstrate segmentation-based editing by removing objects from the segmentation maps. (a) represents the original segmentation map, while (b) shows the generated image by AM-Adapter following the target structure of (a). (c) and (e) are edited segmentation maps derived from (a) with specific modifications, such as modifying or removing the colors of specific instances within

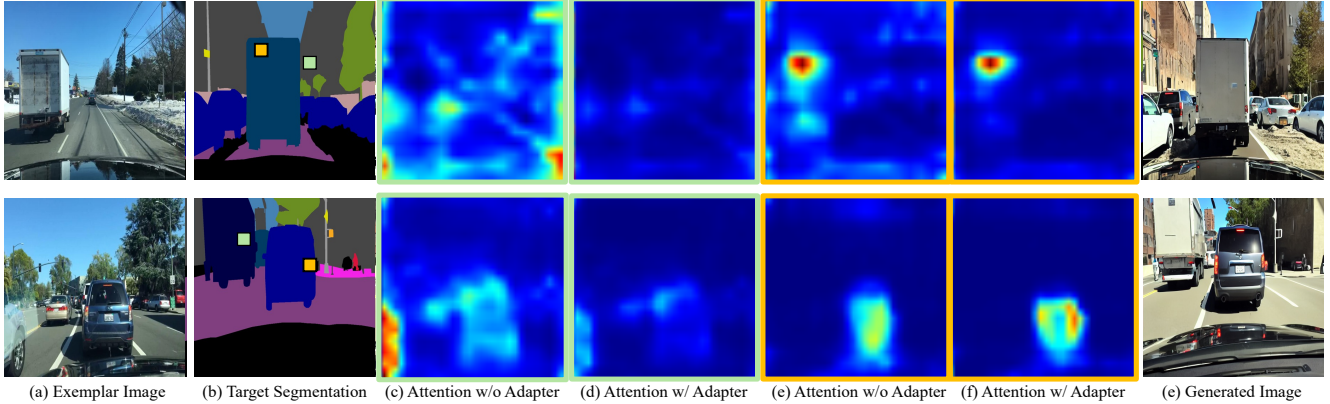


Figure 12. **Additional Attention Visualization:** (a) Exemplar image with desired appearance, (b) target segmentation with desired structure, and (g) generated image. Green and orange markers in (b) indicate query points. (c) and (d) show the augmented self-attention map $Q_i^Y (K_i^X)^T$ from the green marker, before and after applying AM-Adapter, respectively. (e) and (f) show the augmented self-attention map $Q_i^Y (K_i^X)^T$ from the orange marker, before and after applying AM-Adapter, respectively.

the map to adjust the semantic information. For example, in the first row, (c) removes the vehicles in the center, while (e) removes the buildings on the left. In the second row, (c) eliminates the traffic lights and trees, while (e) removes the person. (d) is the generated image by AM-Adapter following the target structure of (c), while (f) is the generated image by AM-Adapter following the target structure of (e).

Figure 20, in contrast, showcases segmentation-based editing through object addition in the segmentation maps. (a) depicts the edited segmentation maps from Figure 19 where specific objects were removed, forming the basis for subsequent augmentation, and (b) presents the image generated based on (a). (c) and (e) illustrate segmentation maps augmented by introducing additional semantic instances to enrich the scene. For example, in the first row, (c) introduces pedestrians into the left side of the scene, while (e) adds buildings to the background. In the second row, (c) incorporates a vehicle into the scene, while (e) includes pedestrians. The resulting images, generated based on these augmented segmentation maps, are depicted in (d) and (f), highlighting the model’s capability to seamlessly integrate new objects into the scene while preserving global consistency.

The results shown in Figure 19 and Figure 20 highlight the versatility of AM-Adapter in addressing diverse semantic editing tasks, including object removal and addition. The method effectively synthesizes images that reflect both the structural modifications and the appearance of exemplar, showcasing its potential for downstream applications such as semantic image editing [21]. These findings further validate AM-Adapter’s contribution to advancing exemplar-based semantic image synthesis.

D.2. Image-to-Image Translation

In Figure 21, we present the results of AM-Adapter in image-to-image translation. The first and third rows show case exemplar images representing a diverse range of weather conditions and times of day. The second and fourth rows illustrate the generated results, where the detailed appearance of the exemplar image is seamlessly transferred into the desired structure of the given target segmentation map. Notably, even within the same category, subtle variations exist. For instance, sunny conditions can vary between partly cloudy and completely clear skies, the sky can display different hues during sunset, and night scenes can have varying levels of brightness. Describing such nuanced differences using textual descriptions is inherently challenging. By using exemplar images to replace ambiguous textual descriptions, AM-Adapter can translate the appearance of the given image into the user-intended local exemplar appearance, with segmentation maps serving as anchors.

D.3. Appearance-Consistent Consecutive Video Frame Generation

As illustrated in Figure 22, AM-Adapter effectively generates appearance-consistent consecutive video frames when provided with the target segmentation maps for each frame and a single exemplar image. The first row depicts the target segmentation maps of consecutive frames provided by the BDD100K [42] dataset, arranged in temporal order from left to right, while the second row shows the corresponding generated images that reflect the structure of each target map.

It is critical to note that, as mentioned in Section 3.5, our method was trained using pairs of images generated by applying random augmentations, such as flipping and cropping, to a single anchor image. This training process was designed to facilitate local appearance transfer, with-

out explicitly considering inter-frame continuity or consistency. Nevertheless, our method effectively transfers the appearance of the exemplar image, resulting in consecutive frames that maintain appearance consistency. These results indicate that the performance of our model could be further refined by fine-tuning with video-image and segmentation pairs explicitly designed to ensure temporal consistency.

E. Limitation and Discussion

Dependency on Pretraining. As discussed in Section 3.5, our training process is divided into two stages: ControlNeXt [29] for generation and AM-Adapter for matching. In the first stage, ControlNeXt learns to generate realistic images using segmentation maps as conditions. However, if ControlNeXt fails to adequately learn the generative capabilities or fully grasp the semantic information from the segmentation maps, it can negatively affect the performance of the learnable matching cost in AM-Adapter, since it is learned in a data-driven manner using segmentation-image pairs. This underscores the importance of robust pre-training for ControlNeXt.

Limited Temporal Consistency Under Large Scene Changes. In Figure 22 and Section D.3, we demonstrated our method’s ability to generate appearance-consistent frames using an exemplar image and the target segmentation maps of consecutive video frames as input. However, when there are substantial scene changes (e.g., large camera motion), the consistency between generated frames diminishes.

As mentioned in Section D.3, this limitation arises from our training approach, which uses pairs of randomly augmented images derived from a single anchor image. While this method effectively accounts for spatial differences within a pair of frames, it does not address temporal consistency across frames, resulting in temporally inconsistent images during large scene transitions. To overcome this limitation, fine-tuning the adapter with video data that explicitly incorporates temporal consistency during training could enhance its ability to generate consistent frames, even under significant scene variations.

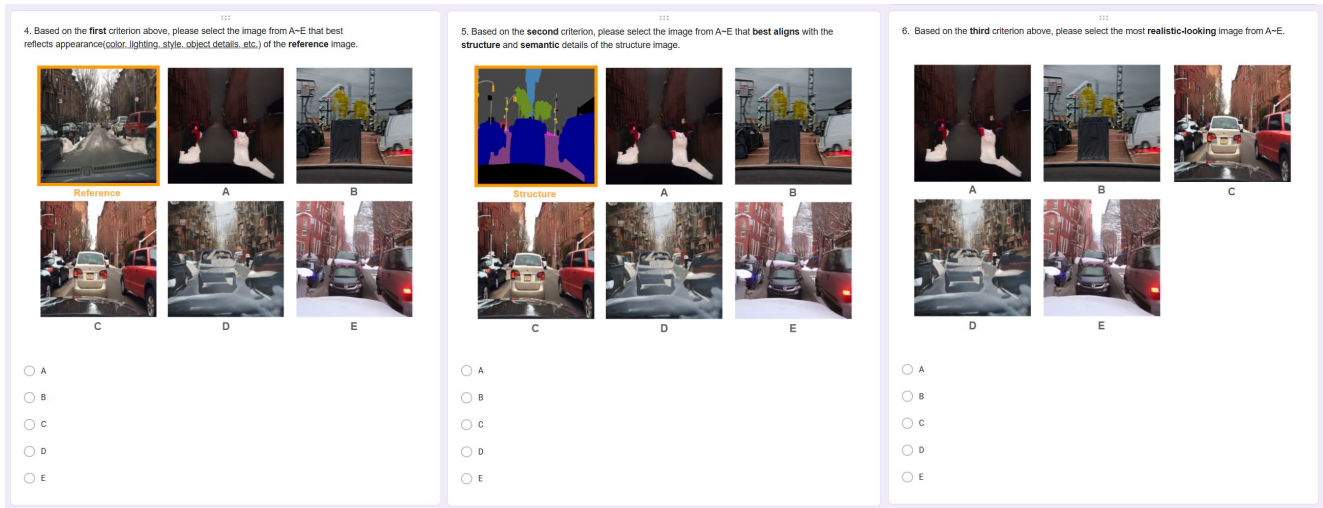


Figure 13. **An Example of a User Study Comparing AM-Adapter with Previous Methods.** For structure preservation, we provide the target segmentation map and generated images from different methods, ControlNet [43] + IP-Adapter [41], FreeControl [23], Cross-Image Attention [1], Ctrl-X [18] and AM-Adapter. For appearance preservation, we provide the exemplar image and the generated images from those methods. For image quality, we compare solely the generated images. For a fair comparison, we randomly select the sample generated from exemplar-segmentation pairs from a large pool.

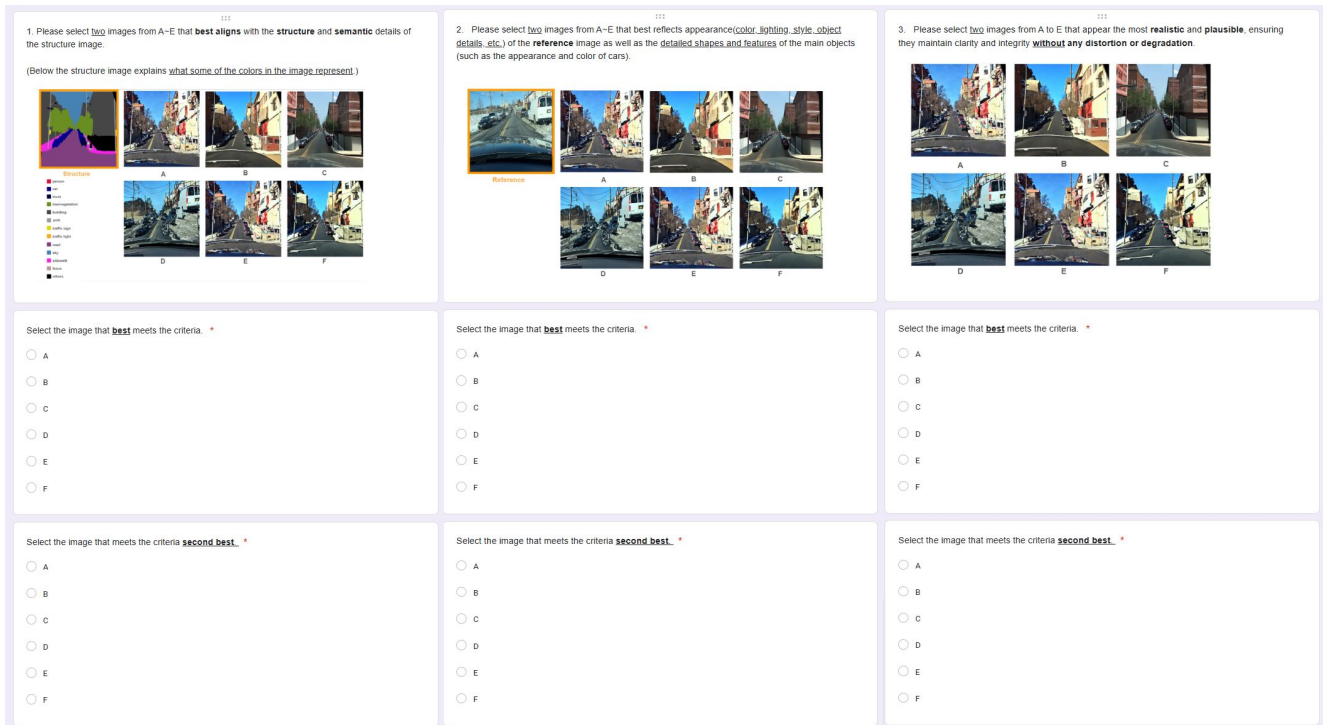


Figure 14. **An Example of a User Study Comparing AM-Adapter with Ablation Studies.** For structure preservation, we provide the target segmentation map and generated images from different methods, key-value replacement (MasaCtrl [2]), DreamMatcher [26], augmented self-attention, augmented self-attention w/ finetuning, augmented self-attention + categorical matching cost, and **AM-Adapter**. For appearance preservation, we provide the exemplar image and the generated images from those methods. For image quality, we compare solely the generated images. For a fair comparison, we randomly select the sample generated from exemplar-segmentation pairs from a large pool.



Figure 15. **Additional Qualitative Results of AM-Adapter.** Visualization of results generated by **AM-Adapter (Ours)** across various scenarios.

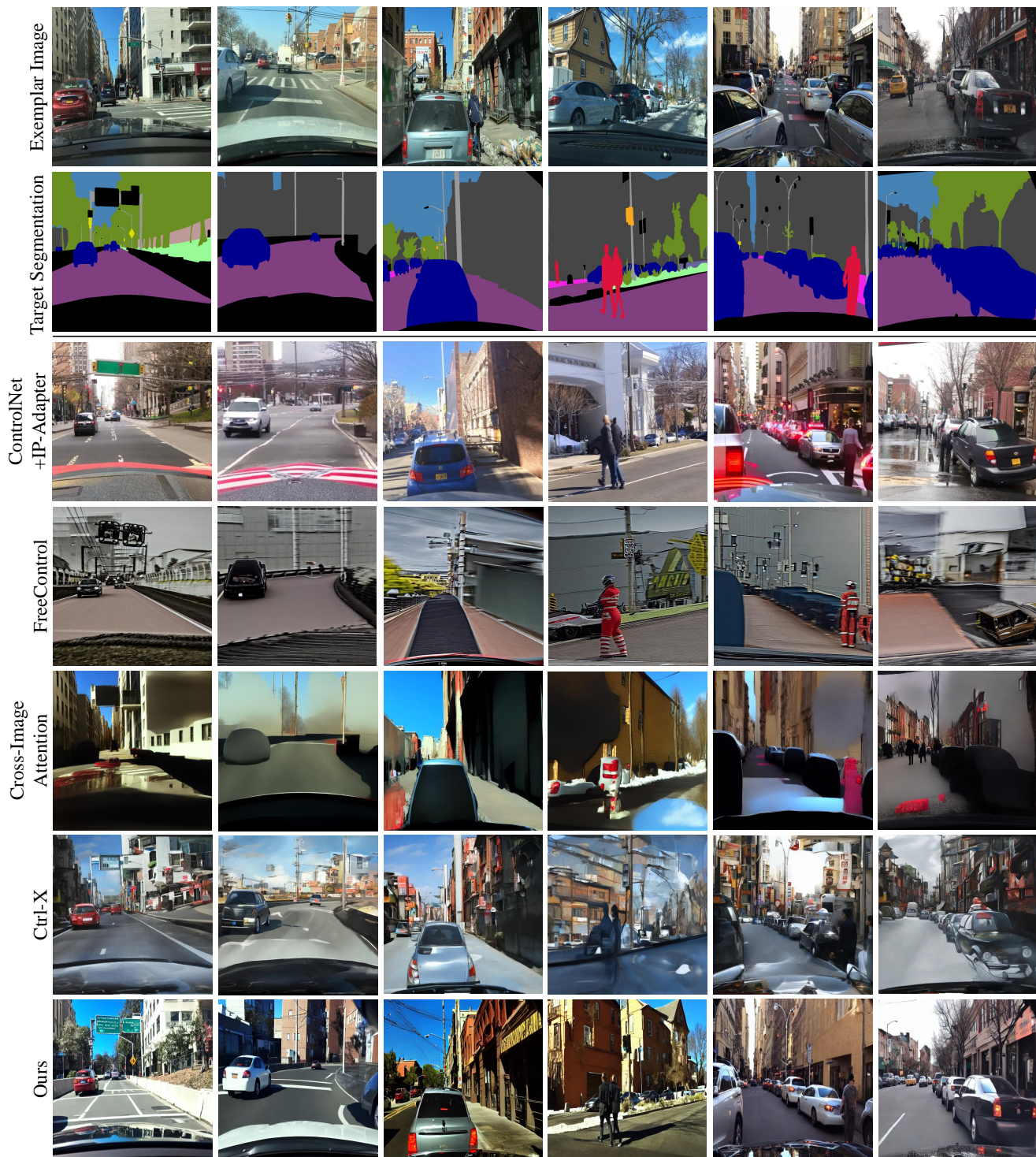


Figure 16. **Qualitative Comparison with Other Methods.** Additional qualitative comparison on BDD100K [42] dataset with previous methods, including ControlNet [43] + IP-Adapter [41], FreeControl [23], Cross-Image Attention [1] and Ctrl-X [18].

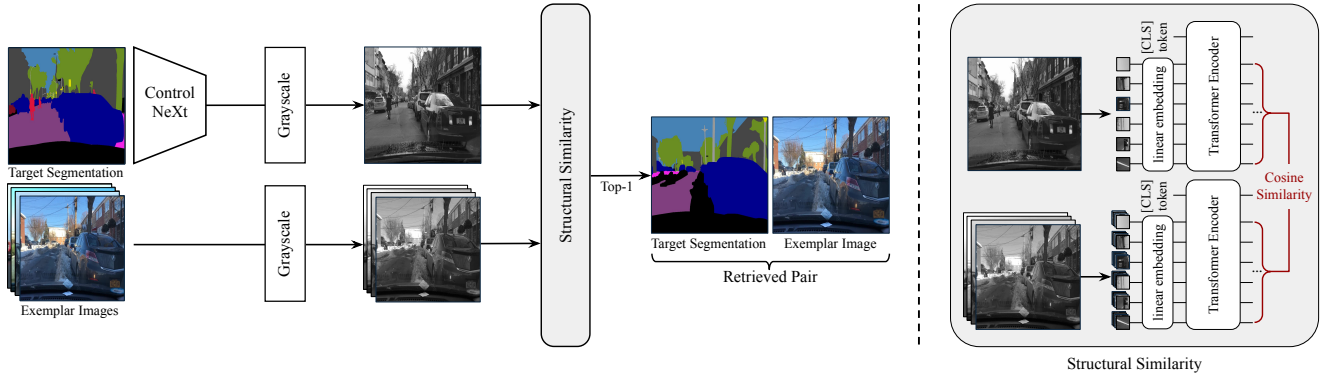


Figure 17. **Details of the Retrieval-based Inference.**



Figure 18. **Retrieval Examples.** During inference, our retrieval technique selects the exemplar image that exhibits the highest structural similarity to the target segmentation map.

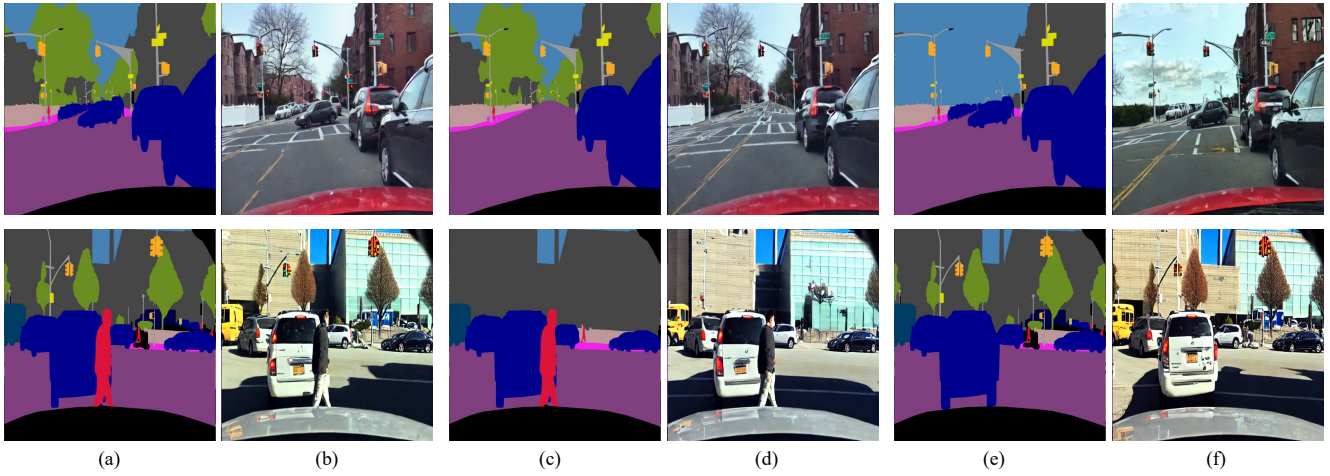


Figure 19. **Application: Object Removal by Segmentation-Based Editing.** (a) Original target segmentation with desired structure, (b) generated image given the target segmentation map (a), (c) edited target segmentation map, (d) generated image given the target segmentation map (c), (e) edited target segmentation map, (f) generated image given the target segmentation map (e).

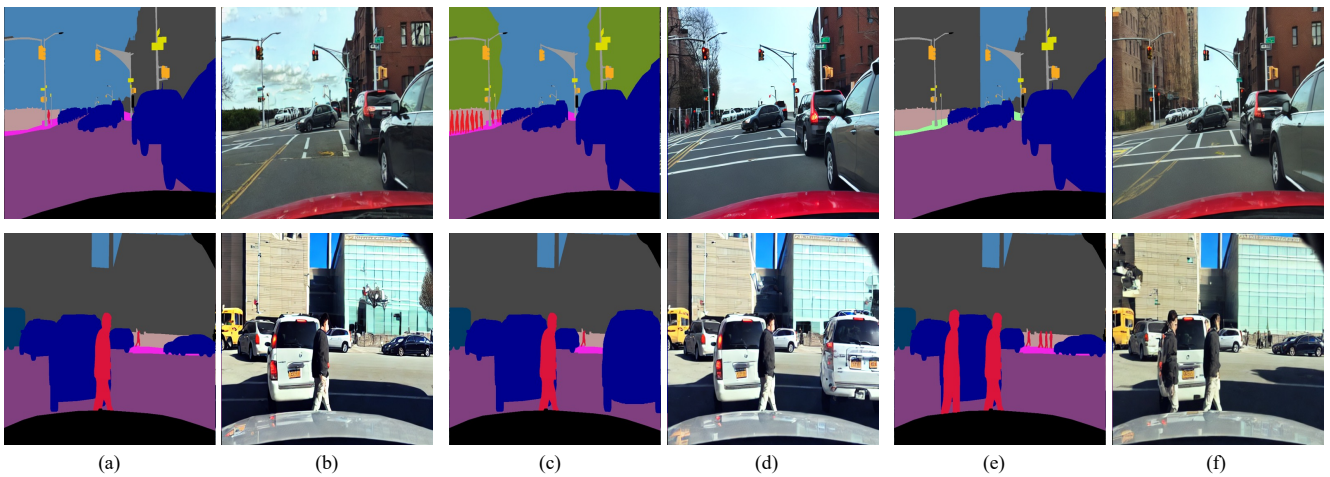


Figure 20. **Application: Object Addition by Segmentation-Based Editing.** (a) Edited target segmentation with desired structure, (b) generated image given the target segmentation map (a), (c) edited target segmentation map, (d) generated image given the target segmentation map (c), (e) edited target segmentation map, (f) generated image given the target segmentation map (e).

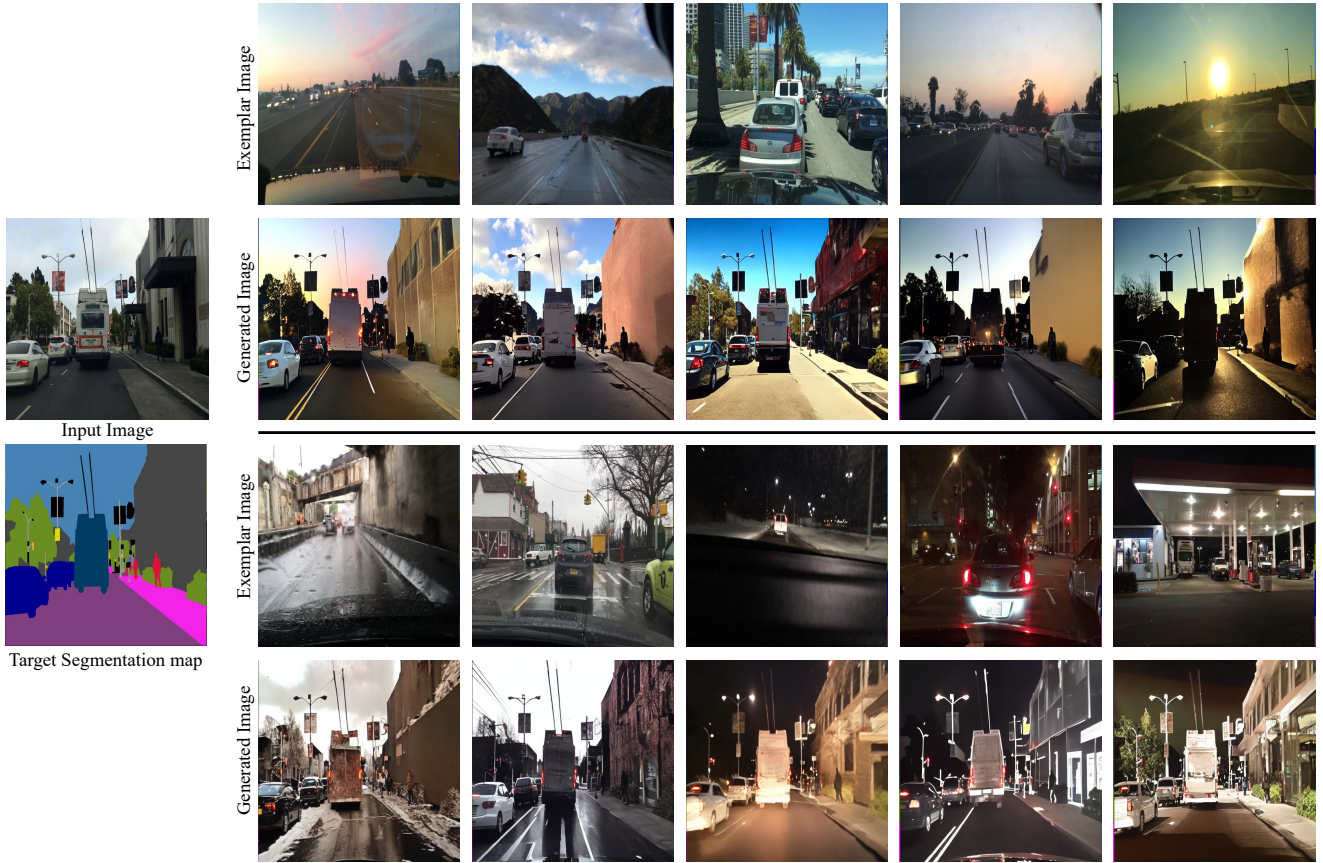


Figure 21. **Application: Image-to-Image Translation.** The first and third row represent exemplar images reflecting various weather conditions and times of day, including various categories such as cloudy days, sunset hours, sunny, night, and rainy conditions. The second and fourth rows depict the resulting images that incorporate the structure of the target segmentation along with each exemplar image.

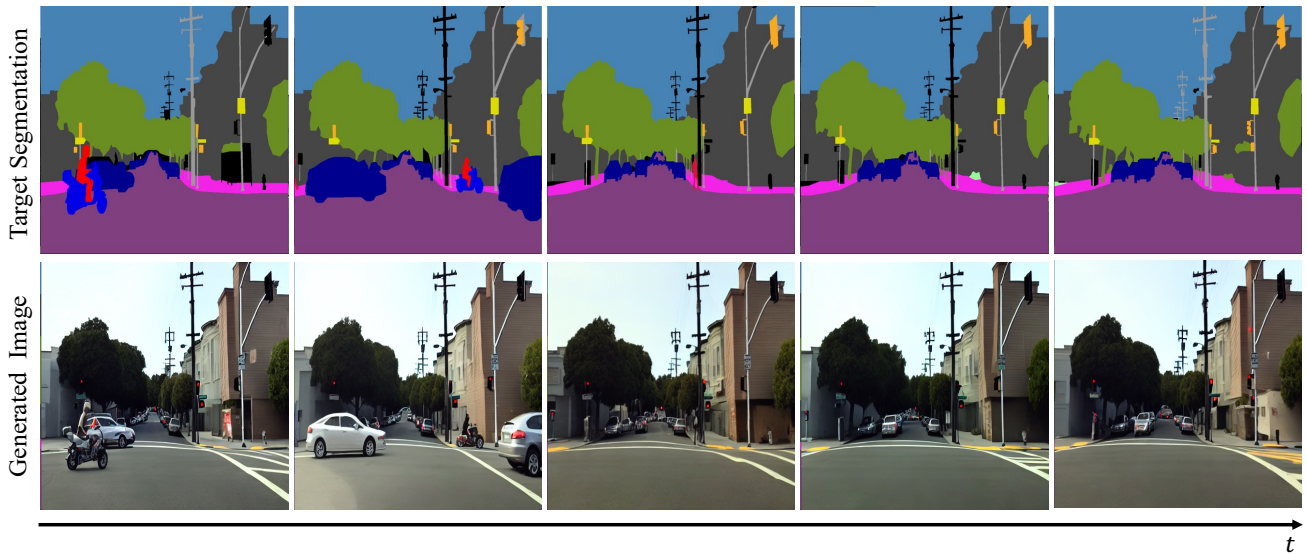


Figure 22. **Application: Appearance-Consistent Consecutive Video Frame Generation.** The target segmentation maps in the first row are consecutive frames provided by the BDD100K [42] dataset. The second row displays the generated image results corresponding to each target segmentation maps. The frames are arranged sequentially from left to right.